The Effect of Head Rotation on the Geometry and Hemodynamics of Healthy Vertebral Arteries

NICOLAS ARISTOKLEOUS [ID],[1] IOANNIS SEIMENIS,[2] GEORGIOS C. GEORGIOU,[3] ANDREW NICOLAIDES,[4] and ANDREAS S. ANAYIOTOS[1]

[1]Department of Mechanical Engineering and Materials Science and Engineering, Cyprus University of Technology, 45 Kitiou Kyprianou Str., Dorothea Bldg, 5th Floor, 3041 Limassol, Cyprus; [2]Laboratory of Medical Physics, Medical School, Democritus University of Thrace, Xanthi, Greece; [3]Department of Mathematics and Statistics, University of Cyprus, Nicosia, Cyprus; and [4]Department of Vascular Surgery, Imperial College, London, UK

Associate Editor Jane Grande-Allen oversaw the review of this article.

Abstract—The geometric and hemodynamic characteristics of the left and right vertebral arteries (LVA, RVA) of six healthy volunteers were investigated for the supine (*S*) and the prone position (*P*) a common sleeping posture with head rotation. MRI images were used to reconstruct the subject specific three-dimensional solid models of the LVA and RVA from the level of the carotid bifurcation to the vertebrobasilar junction (VJ). Geometric parameters such as cross sectional area ratio, curvature, tortuosity and branch angle were estimated. MR-PCA was used to obtain the blood flow waveforms for the two positions and computational fluid dynamics (CFD) were used to assess the flow field in terms of wall shear stress (WSS) relative residence times (RRT) and localized normalized helicity (LNH). Significant geometric changes but moderate flow changes were observed for both vertebral arteries with head rotation. The CFD results at the VJ show that head rotation causes changes in the WSS distribution, RRT and LNH. Further studies are warranted to assess the clinical significance of the results in terms of atherosclerosis development at the VJ and how the observed geometric changes may affect blood flow to the brain in healthy subjects and vertebral artery stenosis patients, and in terms of increased rapture susceptibility in vertebrobasilar aneurysm patients.

Keywords—Vertebral artery, Posture changes, Atherosclerosis, Imaged-based CFD.

INTRODUCTION

The vertebral arteries (VAs) and internal carotid arteries (ICAs) are the four major arteries supplying the brain circulation through the circle of Willis.[6] The confluence of the left and right VAs as they ascent towards the base of the brain give rise to the basilar artery (BA) at the base of the pons which is part of the posterior cerebral circulation. The BA is the only large artery in which two arterial flows merge.[15]

In healthy adults, the left vertebral artery (LVA) is dominant in about 50% of the total population, the right vertebral artery (RVA) in about 25% and in the remaining ~25% of the total population the two VAs are of approximately similar size.[9] Hong *et al.* claim that this flow inequality of the VAs contributes to BA curvature and towards the development of peri-vertebrobasilar junctional infarcts.[15] Ravensberger *et al.* report that the combined role of VJ geometry and local hemodynamics may contribute to the development in atherosclerosis at this location.[29]

In ischemic stroke patients, stenotic lesions in both extracranial and intracranial segments of the VAs account for about 25% of all lesions, while VA constitutes the second most common site of stenosis after ICA.[9] The same investigators have also indicated that in patients with posterior circulation stroke or transient ischemic attack, about 20% of patients have more than 50% VA stenosis. Aneurysms located at the VJ have also been reported, as lesions often associated with fenestration of the proximal BA. Most patients present with subarachnoid hemorrhage and are treated with endovascular procedures.[1,27]

The geometric and hemodynamic characteristics of the carotid arteries, which constitute the main neck arteries, have been the topic of previous investigations that focus on the role of hemodynamic parameters in the development of arterial disease. It has been claimed

Address correspondence to Nicolas Aristokleous, Department of Mechanical Engineering and Materials Science and Engineering, Cyprus University of Technology, 45 Kitiou Kyprianou Str., Dorothea Bldg, 5th Floor, 3041 Limassol, Cyprus. Electronic mails: n.aristokleous@cut.ac.cy and n.aristokleous@dundee.ac.uk

that low and oscillating wall shear stress is involved in promoting atherogenesis as evidenced by the prevalence of atherosclerotic plaques at the site of the carotid bifurcation.[17,18,21,29,30] Furthermore, other investigators have stressed the importance of head and neck posture changes in the carotid bifurcation pathophysiology *via* the associated geometric morphology and hemodynamic alterations.

Glor *et al.* have highlighted that the carotid bifurcation undergoes motion and posture change and experiences alterations in geometry, and subsequently, in hemodynamics.[13] In previous studies with 10 volunteers, we have shown that torsion of the head with bilateral head rotation causes geometric changes in the carotid bifurcation and subsequent changes in the local hemodynamic flow field.[3,4,26] These changes may be important in the development of atherosclerotic disease and its proliferation, as well as in complications in cases of significantly stenotic or stented vessels with total occlusion or kinking.[3,26] Aristokleous *et al.* 2014, report that the geometric changes in the carotid bifurcation due to head rotation alter the spatial and temporal distribution of specific hemodynamic parameters, such as normalized oscillatory shear index (nOSI), relative residence time (RRT) and helicity (HL), that have previously been associated positively or negatively with the development of atherosclerotic disease.[4,10,18,20,21] The same authors suggest that an individualized approach is required to fully assess the postural role in atherosclerosis development and in possible geometric complications arising in stenotic and stented vessels.

In view of the above findings for the carotids and given the significant intra- and inter-subject cross-sectional variation between the LVA and the RVA and the associated flow inequality,[3] it is important to investigate if head rotation causes changes in the geometry of the extracranial and intracranial sections of the VAs. Furthermore, as the VJ geometry plays a significant role in the local hemodynamics, and possibly atherosclerotic development as reported by other investigators,[29] there is a need to study VA hemodynamic changes associated with head posture and their role in atherogenesis.

Therefore, the present study aims at: (a) investigating and assessing potential morphology changes in the geometry of the VAs from the level of the carotid bifurcation divider up to the VJ between the supine head posture and the prone head posture with neck rotation. The latter is a customary sleeping posture of many individuals and it may expose the vertebrals to a geometric change for an extended time period, whilst it also provides the maximum head rotation achievable in an easy and reproducible manner. (b) Studying the potential impact of head rotation on the VA general blood flow field and on the local hemodynamics at the VJ.

MATERIALS AND METHODS

Study Group

The present study was approved by the Cyprus Bioethics Committee. The group of subjects for the morphology and the blood flow studies consisted of six asymptomatic and presumably healthy men with no evidence of arterial stenosis or any chronic disease (mean age of 30, range 22–39 years). Each participant was imaged in two different scanning sessions corresponding to the two investigated head postures: (1) the supine (*S*) neutral head position; and (2) the prone (*P*) position with rightwards head rotation up to 80°.

MRI Imaging

MRI data were acquired with a 3T system (Achieva, Philips Medical Systems, Best, The Netherlands) using the built-in quadrature body coil for proton excitation. A phased array head-neck coil and a phased array superficial coil were used for signal detection in the supine and prone position, respectively. Anatomical data were obtained with a 3D time-of-flight (TOF) method. For each head posture, careful planning allowed for adequate coverage of both the left and right VAs by using carotid bifurcations (CBs) as reference anatomical landmarks. Anatomical coverage extended from around the level of the fifth cervical vertebrae to about the superior pontine border.

The employed gradient-echo pulse sequence [echo time (TE) = 3.5 ms, repetition time (TR) = 23 ms, flip angle (FA) = 20°, $0.36 \times 0.36 \times 1.2$ mm^3 acquisition voxel] provided 100 axial, overlapping (by 50%) slices with a reconstruction voxel of $0.2 \times 0.2 \times 0.6$ mm^3. Variable FA and gradient first moment nulling techniques were implemented to decrease saturation effects of inflowing blood and reduce signal loss due to complex flow respectively. A peripheral pulse triggered, two-dimensional (2D), phase sensitive pulse sequence was employed to acquire flow data spread in 20 phases over the cardiac cycle. The gradient echo sequence used (TE = 13 ms, TR = 20 ms, FA = 10°, $0.35 \times 0.35 \times 5.0$ mm^3 acquisition/reconstruction voxel) provided magnitude and phase-difference, velocity-encoded images using a view sharing reconstruction. An independent scan was prescribed for each VA in both head positions to ensure that the measurement slice was always perpendicular to the flowing blood and at the level of approximately 10 mm above the ipsilateral CB. Optimum encoding velocity per scan was decided upon trial runs.

Surface Reconstruction and Geometric Quantification

Realistic 3D surface models of the VAs were reconstructed from the acquired anatomical MR images using manual segmentation performed with the ITK-Snap (PICSL, USA) software.[34] The reconstructed 3D

lumen surface was further processed using the vascular modeling toolkit (VMTK) in order to smooth, add cylindrical extensions to ensure fully developed velocity profiles and clip the surfaces at specific locations. For global comparison, models were clipped at two sites: (a) 40 mm above and below the ipsilateral carotid bifurcation (Figs. 1a and 1b) 20 mm from both sides of the VJ. The unsmoothed full models of the reconstructed arteries for the two investigated head postures of one volunteer, which include both studied segments, are presented in Fig. 1b. Geometric measures were obtained using the lumen centerlines based on Voronoi diagrams, an approach used widely in bifurcation geometry evaluation[2,33] and implemented in VMTK. Graphical representation of some of the geometric parameters assessed at the VJ is provided in Fig. 1c.

Specifically, tortuosity (T) was calculated as:

$$T = L/D - 1, \qquad (1)$$

where L is the path length of the centerline between the origin and the end of the branch, and D is the Euclidean distance between them. Curvature is defined as the reciprocal of the radius of the local osculating circle and it measures the rate of change in the tangent vector orientation along the curve.[3,12] Curvature data are provided as average values for the segment of interest of each vessel. Bifurcation angle is the angle between the projections of LVA and RVA vectors on to the bifurcation plane. LVA angle is the angle between the projections of BA and LVA on to the bifurcation plane. Planarity angle is the angle between the out of plane components of the BA and LVA vectors. In plane asymmetry angle is defined as the difference between two angles, the angle between LVA and BA and the angle between RVA and BA. The reproducibility and accuracy in the extraction of such geometric parameters have been previously estimated.[3] Vertebral artery cross sectional areas were calculated
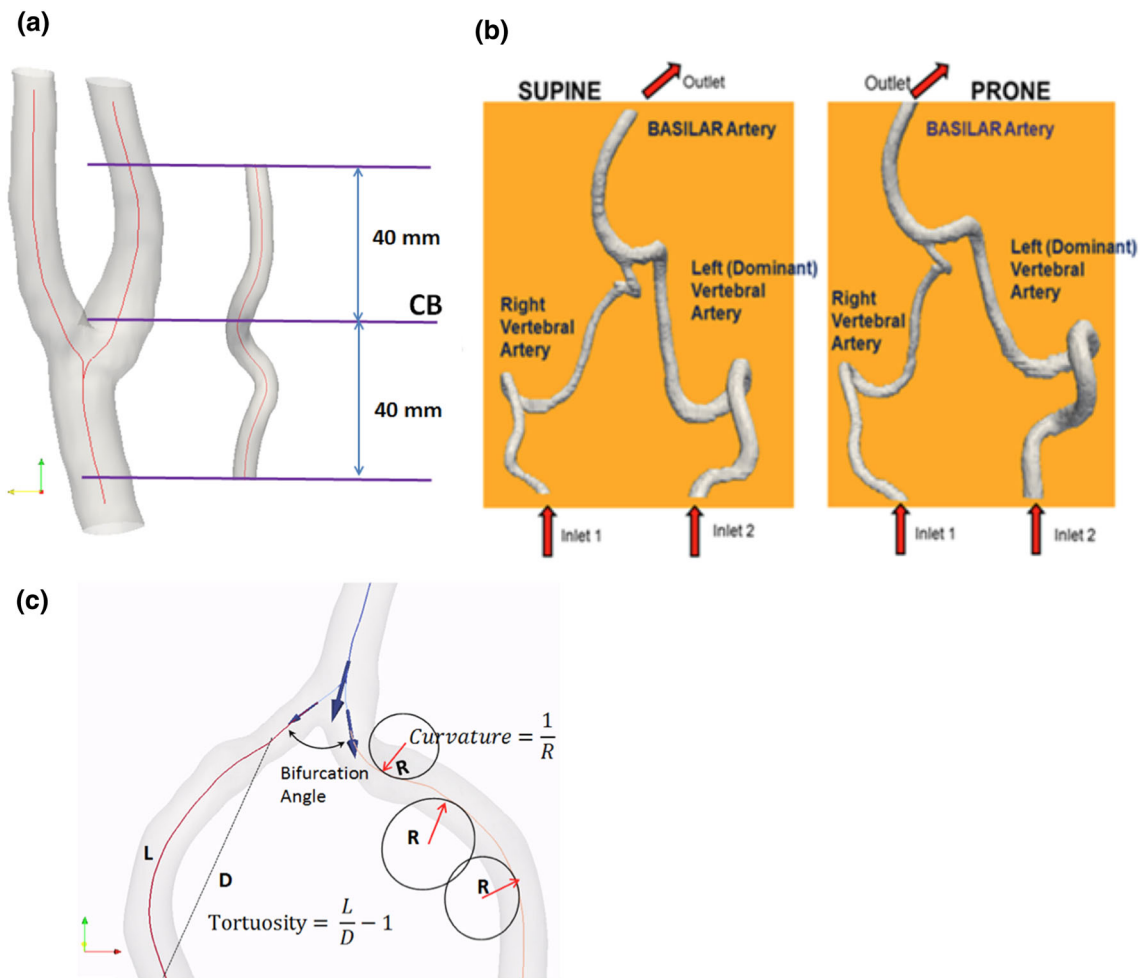

FIGURE 1.   a. Frame of reference for comparable results at the extracranial segment of the vertebral artery studied. b The unsmoothed full models of the reconstructed arteries for the two investigated head postures. c Graphical representation of some of the geometric parameters assessed at the vertebrobasilar junction (L: Centerline's path length, D: Euclidean distance, R: Radius of the local osculating circle).

from the velocity-encoded images which were obtained as thick transverse sections (5 mm) vertical to the vessel's centerline at the acquisition level (i.e., 10 cm above the ipsilateral carotid bifurcation). Presented areas represent average values over the entire cardiac cycle since the calculated areas corresponding to the 20 acquired cardiac phases were averaged. In this respect, estimated areas partly compensate for positional uncertainties and cardiac phase variations.

Flow Waveforms

Blood flow time history was obtained by integrating the through-plane velocity over the lumen cross-sectional area at each cardiac phase using Segment v1.9 R2178 (Medviso AB).[14] To normalize our results at the same heart rate (HR), all blood velocities and flow rates were scaled at a constant HR of 60 bpm according to:

$$V_{\text{scaled}} = V_{\text{measured}} \left(\frac{60}{HR_{\text{measured}}} \right), \quad (2)$$

where V represents blood velocity.

Computational Simulations

Computational fluid dynamics (CFD) analysis was performed on imaging data acquired from four volunteers. In one volunteer LVA was dominant over RVA, in another RVA was dominant over LVA and in the rest two cases LVA and RVA were approximately equally sized in terms of cross section. Thus, all possible scenarios regarding VA dominance were simulated. The two models of each volunteer, corresponding to the supine and prone postures respectively, were used for numerical simulations under pulsatile conditions at the vertebrobasilar artery junction.

The CFD simulations were based on the following modeling assumptions: (a) blood was considered Newtonian (ρ 1050 kg/m^3, μ 0.0035 kg/m s); (b) the artery wall rigid; and (d) the inlet flow fully developed and laminar. Furthermore, traction-free conditions were applied at the outlet. The impact of these assumptions in computed hemodynamics has been previously discussed extensively.[16,23,24,32]

Meshes of approximate 2.2×10^6 size were constructed by ICEM-CFD v12.1 (Ansys Inc.). More details on meshing are provided elsewhere.[4] The numerical solution was obtained by Fluent v12.1 (Ansys Inc.) by applying the pulsatile Womersley solution on each inlet boundary condition. The realistic inlet velocity waveforms acquired by phase sensitive MRI were decomposed in 15 harmonics with fast Fourier transform using Matlab R2012b (The MathWorks Inc.). The averaged Reynolds number was $Re_{\text{avg}} = 125$ and at peak systole $Re_{\text{peak}} = 450$ and the Womersley number for each inlet

boundary condition based on inlet radius was $2.5 \leq a \leq 4$. A second-order upwind scheme was applied for the discretization of the momentum equations and a second-order interpolation scheme for pressure. A time step of 2.5×10^{-4} s and 4000 iterations per cycle were used in all simulations. The SIMPLEC algorithm was used for pressure–velocity coupling. A time periodic solution was achieved after four flow cycles. Data from the 5th cycle were used to avoid transient effects in the initial cycles. Hemodynamic parameters, such as time-averaged WSS (WSS_{avg}), RRT and localized normalized helicity (LNH) were computed as follows.[11,12,20]

$$WSS_{\text{avg}} = \frac{1}{T} \int_0^T |\boldsymbol{WSS}| \mathrm{d}t, \quad (3)$$

$$RRT = \frac{T}{\left| \int_0^T \boldsymbol{WSS} \cdot \mathrm{d}t \right|}, \quad (4)$$

$$LNH = \frac{\boldsymbol{v} \cdot \boldsymbol{\omega}}{|\boldsymbol{v}||\boldsymbol{\omega}|}, \quad -1 \leq LNH \leq 1, \quad (5)$$

where T is the cardiac cycle period, $\boldsymbol{v}$ the velocity vector and $\boldsymbol{\omega}$ the vorticity vector. RRT represents a combination of low and oscillating WSS and is an indicator of unfavorable hemodynamic conditions for the experiencing arterial walls.[20] In contrast, HL acts to suppress flow disturbances, thus it is supposed to prevent plaque deposition.[11] As proposed by Morbiducci *et al.*,[22] the sign of LNH is related to the rotational direction of intravascular fluid structures and, thus, positive and negative values characterize clockwise and counterclockwise rotation, respectively.

Statistical Analysis

Statistical analysis was performed using R.[28] Data are presented as mean values with standard deviation (SD). The Wilcoxon signed–rank test was used for comparisons between the prone and supine positions. For comparisons between the left and right VAs, the Wilcoxon rank sum test (Mann–Whitney test) was used. $p < 0.05$ was considered to indicate significance and, therefore, only p values < 0.05 are denoted.

RESULTS

The reconstructed 3D surface models corresponding to the extracranial segment of the VA were clipped 40 mm above and 40 mm below the ipsilateral carotid bifurcation, as illustrated in Fig. 1a. The red line indicates the centerline along which curvature and tortuosity were calculated. The full unsmoothed models, which also incorporate the VJ segment used for CFD simulations, are
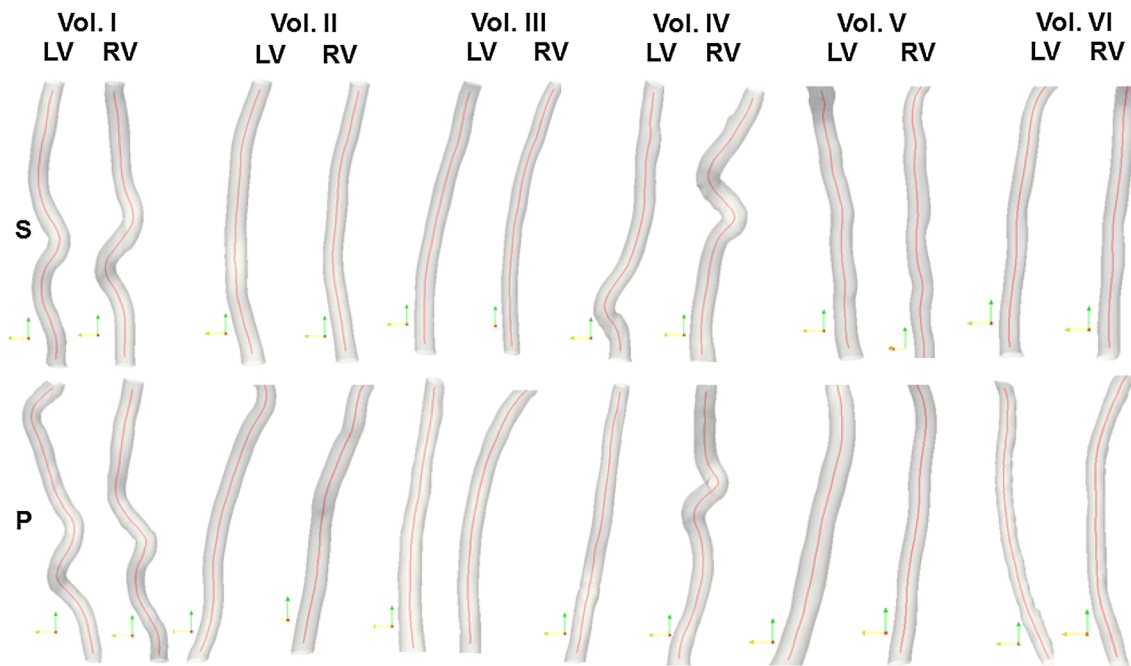
FIGURE 2. Reconstructed 3D models for left and right vertebral arteries (LV, RV) for the six volunteers (Vol. I-VI). The top row shows the models for the supine posture (*S*) and the bottom row the respective models for the prone posture with rightward head rotation (*P*). The segments were clipped at ±40 mm from the corresponding carotid bifurcation level. Red line indicates lumen centerline.

TABLE 1. Individual geometric parameters at supine (*S*) and prone (*P*) head postures for the right (RVA) and the left (LVA) vertebral artery segments at the level of the carotid bifurcation divider.

Vol. #	Head position	RVA		LVA	
		Curvature (1/mm)	Tortuosity	Curvature (1/mm)	Tortuosity
I	S	0.094	0.011	0.083	0.071
	P	0.098	0.094	0.104	0.141
II	S	0.022	0.016	0.044	0.029
	P	0.084	0.026	0.047	0.039
III	S	0.025	0.011	0.023	0.018
	P	0.055	0.116	0.027	0.008
IV	S	0.098	0.131	0.067	0.045
	P	0.104	0.139	0.056	0.041
V	S	0.051	0.032	0.064	0.094
	P	0.044	0.095	0.057	0.065
VI	S	0.070	0.119	0.061	0.082
	P	0.056	0.121	0.035	0.023

represented in Fig. 1b. Figure 1c graphically defines some of the geometric parameters assessed at the VJ.

Figure 2 shows the reconstructed 3D models for the LVA and RVA sections at the CB level for the six volunteers studied (Vol. I–VI). The upper row shows the models for the supine head position (*S*) (neutral posture without head rotation), while the lower row represents the corresponding models for the prone position (with rightward head rotation) (*P*). As also indicated by subject-specific curvature and tortuosity data shown in Table 1, head rotation may cause considerable change in the geometric characteristics of the VAs.

Table 1 presents the curvature and tortuosity values for the two head postures of the LVA and RVA for each volunteer separately. Overall, there is no significant difference neither in tortuosity nor in curvature between the left and right VAs in the supine or prone position. Regarding RVA, the results show no change in curvature, but rightwards head rotation results in a significant increase in tortuosity ($p < 0.05$). LVA results exhibit no significant difference between the two head postures.

Table 2 shows the extracted geometric parameters at the VJ for the two head postures. Head rotation is

TABLE 2. Mean values (±SD) of geometric parameters at the supine (*S*) and prone (*P*) head postures for the VA segment at the vertebrobasilar junction.

		S	P	p value
Bifurcation	Angles	47.1 ± 7.2	58.0 ± 7.1	0.07
LVA		21.9 ± 4.0	26.0 ± 4.3	0.94
Planarity		19.1 ± 4.1	13.7 ± 5.7	0.03
Asymmetry		22.1 ± 6.2	17.1 ± 5.6	0.04
Curvature (1/mm)	BA	0.06 ± 0.01	0.07 ± 0.01	1.00
	LVA	0.09 ± 0.04	0.09 ± 0.03	1.00
	RVA	0.09 ± 0.01	0.1 ± 0.02	0.34
Tortuosity	BA	0.06 ± 0.06	0.07 ± 0.05	1.00
	LVA	0.33 ± 0.4	0.34 ± 0.5	0.78
	RVA	0.43 ± 0.6	0.39 ± 0.5	0.38
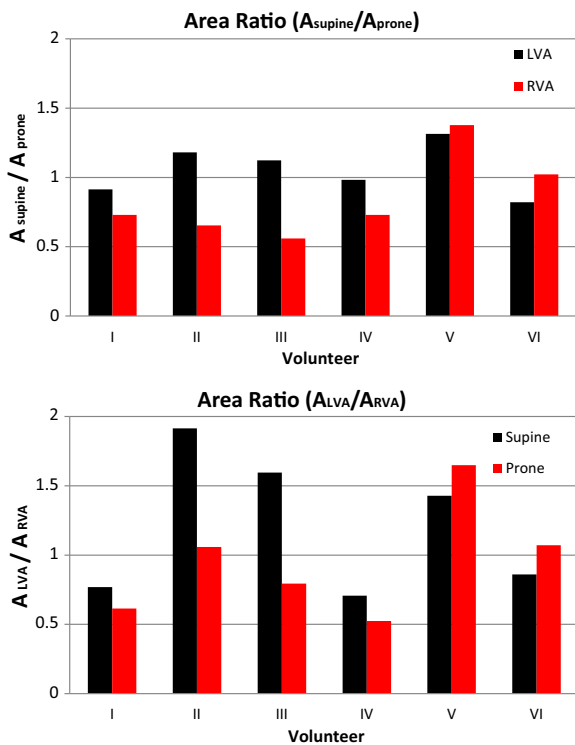
FIGURE 3. Cross-sectional area ratios between LVA and RVA for both head postures (top) and between the two head postures for both vertebral arteries (bottom) for all study volunteers.

not associated with any significant change neither in tortuosity nor in curvature. A decrease in all angles is noted in the prone position, which is significant ($p < 0.05$) for the planarity and asymmetry angles.

The histogram in Fig. 3 (top) illustrates the comparison of cycle-averaged cross-sectional area ratios between supine and prone head postures for the left and right VAs separately. LVA area decreases in three cases with head rotation, while it increases in the rest. Regarding RVA, prone posture was associated with an area increase in the majority of the cases. Overall, no

statistically significant difference was found. The impact of head rotation on the cross sectional areas between the two VAs is presented in Fig. 3 (bottom), where the histogram compares the LVA/RVA area ratios between supine and prone head postures. For the supine posture, the LVA cross sectional area was greater than the RVA area in four cases, whilst in the prone position LVA was greater in three cases. It is worth noting that, in three volunteers, the rightwards head rotation altered the balance between the two arteries, but there was no significant difference in the studied group as a whole.

Figure 4a shows the volumetric cycle-averaged flow rate ratio between LVA and RVA for both head postures. Figure 4b is the corresponding ratio at peak systole. The unequal flow rate ratio between the LVA and the RVA was expected due to their unequal cross sectional areas. For each subject, peak systolic data resemble cycle-averaged data. It is worth noting that only in one case (Vol. VI); rightwards head rotation resulted in significant reallocation of the blood flow between the two arteries. Figure 4c shows the effect of head rotation on the cycle-averaged flow rate ratio Q_{supine}/Q_{prone} for the LVA and the RVA. Figure 4d presents the same corresponding ratios at peak systole. Overall, it is evident that there is a strong inter-subject variation regarding the effect of head rotation on the flow rate within each artery resulting in no significant differences for the whole group.

Figure 5 presents contour plots of cycle-averaged (top row) and peak systolic (bottom row) WSS distributions at the VJ for the supine (left) and prone (right) head postures investigated. A close correspondence between cycle-averaged (top) and peak systolic (bottom) distributions is noted. In the two cases with dominant VA (vol. IV: RVA and vol. V: LVA), rightwards head rotation results in a mild increase in the WSS distribution in the minor VA. For the other two cases with equally sized VAs (vol. II and vol. III), head rotation seems to slightly increase the averaged WSS field at the VJ.
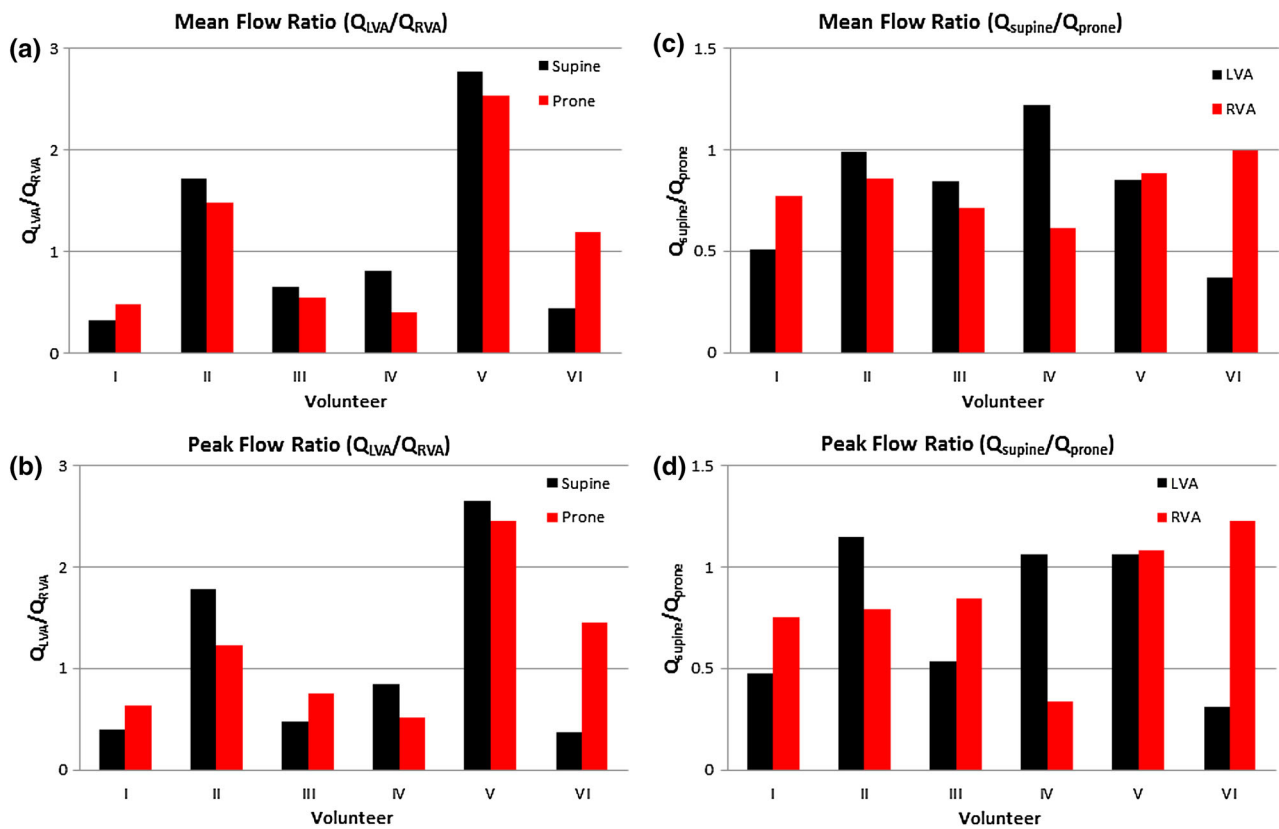
FIGURE 4. Cycle-averaged flow rate ratios between LVA and RVA for both head postures (a) and cycle-averaged flow rate ratios between supine and prone postures for both vertebral arteries (b). Peak flow rate ratios between LVA and RVA for both head postures (c) and peak flow rate ratios between supine and prone postures for both vertebral arteries (d).
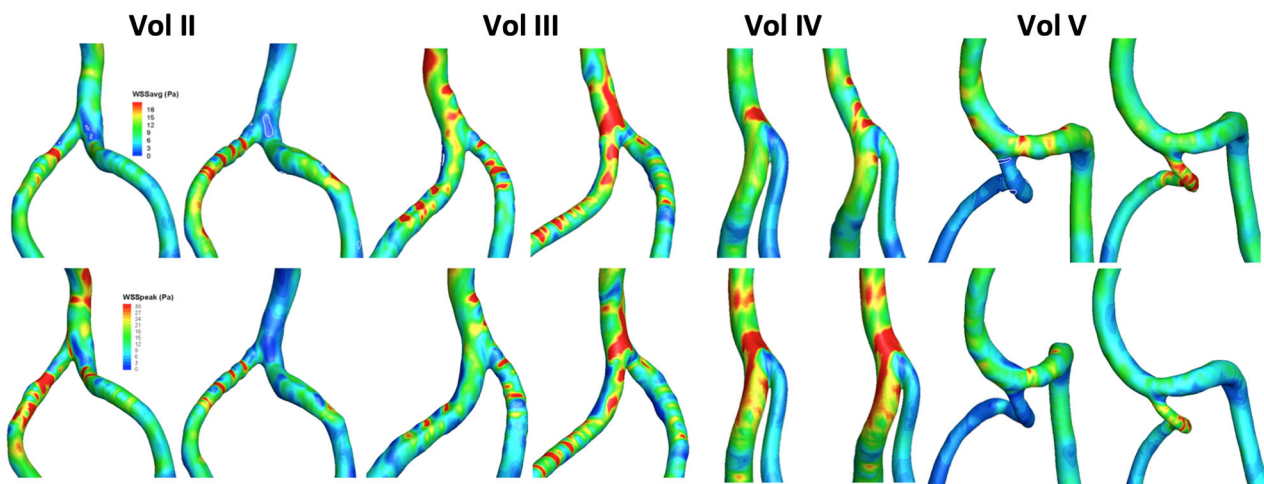

FIGURE 5. Contour plots of cycle-averaged (top row) and peak systolic (bottom row) WSS distribution at the vertebrobasilar junction for the supine head posture (left) and the prone posture with rightwards head rotation (right).

Figure 6 shows the contour plots of RRT distribution at the VJ for the supine head posture (left) and the prone posture with rightwards head rotation (right). It is evident that head position has a limited effect on the RTT distribution at the VJ.

For the two investigated postures, cycle-averaged (top row) and peak systolic (bottom row) isosurfaces of LNH are presented in Fig. 7. Large helical flow structures are observed in the area where the LVA and RVA merge into the BA and continue in high intensity
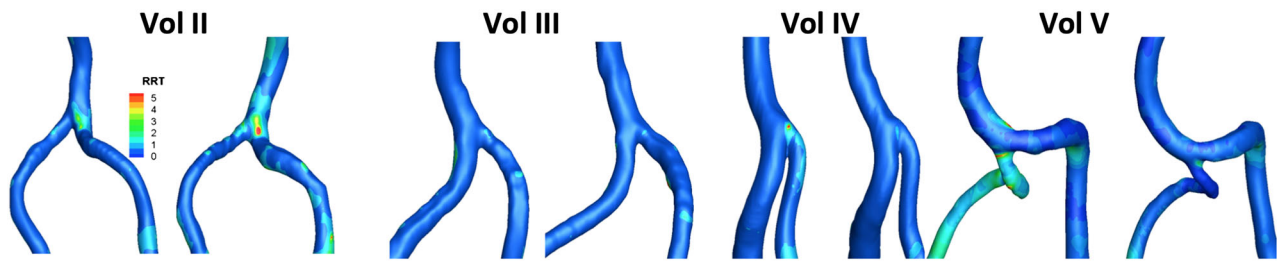
FIGURE 6. Contour plots of RRT distribution at the vertebrobasilar junction for the supine head posture (left) and the prone posture with rightwards head rotation (right).
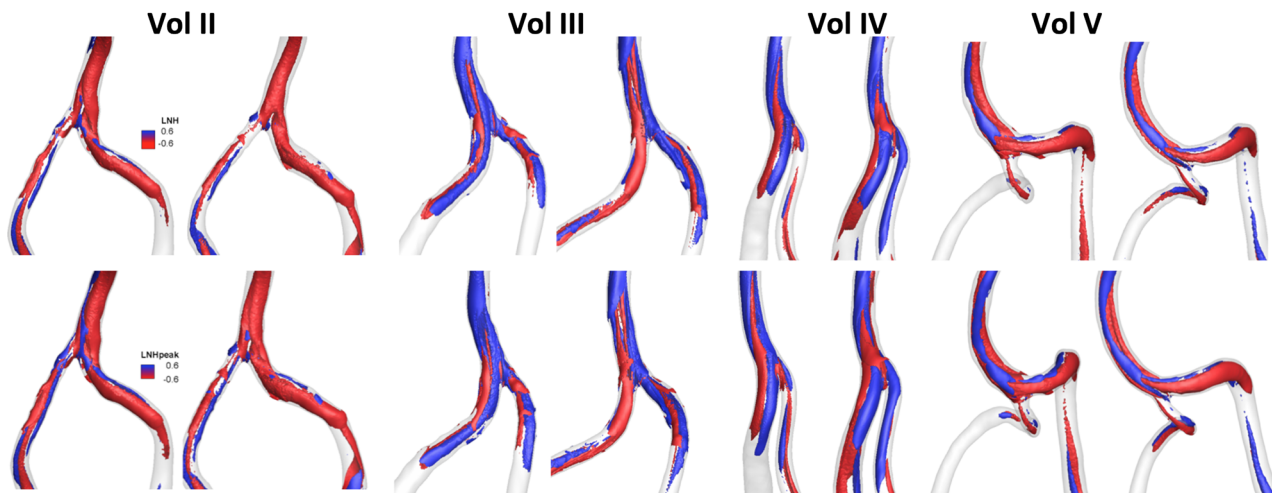

FIGURE 7. Cycle-averaged (top row) and peak systolic (bottom row) localized normalized helicity (LNH) isosurfaces at the vertebrobasilar junction for the supine head posture (left) and the prone posture with rightwards head rotation (right).

and in bidirectional tracts, whilst instantaneous and cycle-averaged spatial extents of LNH are quite similar. Rightwards head rotation in prone position (right) has a minimal effect on blood rotation direction in comparison to normal, supine head posture (left). Prone position, however, seems to be associated with spatial extension of LNH in both VAs.

DISCUSSION

Normal VAs exhibit a high inter-subject variability in terms of origin, morphology, branching and length. The VJ is also characterized by a varied geometry. For an individual geometric configuration of the vertebrobasilar artery system, there may be also considerable differences in the diameter between the left and the right arteries. All these variations may result in significant blood flow differences within the VAs and the VJ,[16] that, in the diagnostic setting, may unsoundly lead to the hypothesis of arterial disease. Presented results suggest that torsion of the neck associated with head rotation may complicate this situation even further by affecting both geometry and blood flow field in VAs.

Geometric changes were observed in the reconstructed geometries of the LVA and RVA, which in some cases were significantly different at the prone position (rightward head rotation) as opposed to the supine position (no head rotation). At the carotid bifurcation level, turning the head to the right seems to have no statistically significant effect on the left VA but it seems to increase the tortuosity of the right VA. With regard to the VA segment at the VJ, however, no consistent changes are observed. Moreover, on an individual basis, there is no correlation in the curvature and tortuosity changes seen between the two VA segments studied. Taking it one step further, the rotation-related change of these two parameters in the extracranial VA segment was compared against the corresponding change in the adjacent common carotid artery and no consistency was observed. Overall, the VA geometric changes due to head rotation are considered to be random and moderate, while there is no predisposition to a specific direction of change for any of the parameters extracted. This variable pattern of change, results from the considerable inter- and intra-subject variability in the baseline geometry of the two VAs, which also holds true for different segments of the same vessel.

Findings of the current study indicate that neck torsion moderately affects cycle-averaged cross-sectional area of VAs, as well as peak blood velocity, albeit in a random fashion. Comparing Fig. 4c and data shown at the top row of Fig. 3, it is observed that although prone posture is associated with a decrease in vessel cross sectional area in five arteries (out of 12 in total), only in one case this results in decreased flow rate. This observation, along with the fact that the shape of the vertebral flow waveform does not change with head posture, suggest that that head rotation may be associated with adjustment of the cross sectional distribution of blood velocities partly compensating for inflicted changes on vertebral cross section.

Using duplex ultrasonography (US), Sakaguchi et al.[31] showed minimal change in extracranial VA flow velocity during neck rotation in the majority of the 1108 subjects studied. In 5% of the cases, the authors found that neck rotation was associated with mechanical compression of the VA, which may lead to vessel injury. The authors concluded that ultrasonography could be useful in identifying vessel compression, especially in patients with symptoms on neck rotation. Synptoms of vertebrobasilar ischemia include dizziness, vertigo, diplopia, blurring of vision, tinnitus and drop attacks. Vertigo or drop attacks are often triggered by neck rotation or extension which produces vertebral artery compression in its bony cervical course.

The variable and possibly significant changes in geometric and blood flow parameters at the prone position found in this study support the suggestion that a personalized diagnostic workup is warranted in symptomatic patients. Since the VAs constitute a major source of cerebral blood flow (CBF), such an individualized approach could also be considered in rapid non-impact head rotation without cervical spine injury, which has been linked to decreased carotid blood flow in an experimental model of reduced CBF.[8]

Observed hemodynamic changes at the VJ, in terms of the three parameters examined (WSS, RRT, LNH), suggest that head posture may affect the developed flow fields and may influence the exposure of vessel walls to significantly different hemodynamic conditions. These changes could be mostly important in the presence of arterial lesions or disease. Rotational vertebral artery occlusion (RVAO) is a rare cause of vertebrobasilar insufficiency that carries a risk of impending stroke. Most patients with RVAO exhibit a stenosis of one VA while the dominant VA is compressed during contraversive head rotation, which compromises the blood flow in the vertebrobasilar region.[5,7] Alteration of local flow fields at the prone position, which is a frequent sleeping posture for many subjects and patients, could have important consequences in the tensile stress distribution around atherosclerotic plaques commonly found at the VJ.[29] Hemodynamic changes in VAs associated with head rotation may also play a role in the subclavian steal syndrome (SSS), which is defined as a group of symptoms that arise from the reversed blood flow in the VA when there is a stenosis in the ipsilateral subclavian artery.[25] The prevalence and impact of this syndrome have been recently reported by Labropoulos et al.[19] Peluso et al.[27] have reported cases of vertebrobasilar aneurysms in patients with fenestration of the proximal BA and evidence of subarachnoid hemorrhage. The possible vessel compression reported by Sakaguchi et al.[31] combined with the geometrical and flowfield changes reported in the present study indicate a possibility of influencing an environment that may favor aneurysmal rapture.

LIMITATIONS

The small sample size of the study group and the limited number of CFD simulations are the main limitations of the current study. Furthermore, the small size of the RVA and LVA cross sections s also another source of error. For area calculations in particular, the in-plane resolution of the acquired velocity-encoded images (0.35 mm^2) resulted in cross-sections with a minimal number of 40 pixels (corresponding to an area of 5 mm^2). Imaging data of higher spatial and temporal resolution could possibly improve robustness of extracted geometrical and blood flow results, respectively. The absence of a suitable vertebral landmark in the extracranial VAs introduces positional uncertainty with regard to geometrical assessment of extracranial segments. The use of the ipsilateral CB as a reference point rather than the relevant VJ aimed at isolating local geometrical changes due to head rotation. An accuracy and reproducibility assessment analysis of the imaging and reconstruction methodology was described in a previous publication.[3] Rigid wall and Newtonian blood fluid assumptions are also considered as limitations associated with the numerical simulations. Further research is required to assess the effects of head rotation in the presence of VA pathology, as well as the role of the hemodynamic parameters examined in the development of VJ stenosis and in the rapture of vertebrobasilar aneurysms.

CONCLUSIONS

This study provides evidence that head rotation may cause moderate to significant geometric changes in the human VAs at the carotid artery bifurcation and VJ levels which are strongly dependent on the individual

vertebrobasilar geometric configuration. These changes may affect the vertebral blood flow field and may have an impact on hemodynamic parameters believed to play an important role in arterial disease development and course. The influence of geometry changes with head rotation warrants further investigation in vertebrobasilar stenosis and vertebrobasilar aneurysm patients.

CONFLICT OF INTEREST

REFERENCES

[1] Albanese, E., A. Russo, and A. J. Ulm. Fenestrated vertebrobasilar junction aneurysm: diagnostic and therapeutic considerations. *J. Neurosurg.* 110:525–529, 2009.

[2] Antiga, L., and D. A. Steimman. Robust and objective decompositionand mapping of bifurcating vessels. *IEEE Trans. Med. Imaging* 23:704–713, 2004.

[3] Aristokleous, N., I. Seimenis, Y. Papaharilaou, G. C. Georgiou, B. C. Brott, E. Eracleous, and A. S. Anayiotos. Effect of posture change on the geometric features of the healthy carotid bifurcation. *IEEE Trans. Inf. Technol. Biomed.* 15:148–154, 2011.

[4] Aristokleous, N., I. Seimenis, G. C. Georgiou, Y. Papaharilaou, B. C. Brott, A. Nicolaides, and A. S. Anayiotos. Impact of head rotation on the individualized common carotid flow and carotid bifurcation hemodynamics. *IEEE J. Biomed. Health Inform.* 18:783–789, 2014.

[5] Brandt, T., and R. W. Baloh. Rotational vertebral artery occlusion: a clinical entity or various syndromes? *Neurology* 65:1156–1157, 2005.

[6] Cebral, J. R., M. A. Castro, C. M. Putman, and N. Alperin. Flow-area relationship in internal carotid and vertebral arteries. *Physiol. Meas.* 29:585–594, 2008.

[7] Choi, K. D., J. H. Choi, J. S. Kim, H. J. Kim, M. J. Kim, T. H. Lee, H. Lee, I. S. Moon, H. J. Oh, and J. I. Kim. Rotational vertebral artery occlusion: mechanisms and long-term outcome. *Stroke* 44:1817–1824, 2013.

[8] Clevenger, A. C., T. Kilbaugh, and S. S. Margulies. Carotid artery blood flow decreases after rapid head rotation in piglets. *J. Neurotrauma.* 32:120–126, 2015.

[9] Cloud, G. C., and H. S. Markus. Diagnosis and management of vertebral artery stenosis. *QJM* 96:27–54, 2003.

[10] Cunningham, K. S., and A. I. Gotlieb. The role of shear stress in the pathogenesis of atherosclerosis. *Lab. Invest.* 85:9–23, 2005.

[11] Gallo, D., D. A. Steinman, P. B. Bijari, and U. Morbiducci. Helical flow in carotid bifurcation as surrogate marker of exposure to disturbed shear. *J. Biomech.* 45:2398–2404, 2012.

[12] Gallo, D., D. A. Steinman, and U. Morbiducci. An insight into the mechanistic role of the common carotid artery on the hemodynamics at the carotid bifurcation. *Ann. Biomed. Eng.* 43:68–81, 2015.

[13] Glor, F. P., B. Ariff, A. D. Hughes, P. R. Verdonck, D. C. Barratt, A. D. Augst, S. A. Thom, and X. Y. Xu. Influence of head position on carotid hemodynamics in young adults. *Am. J. Physiol. Heart. Circ. Physiol.* 287:H1670–H1681, 2004.

[14] Heiberg, E., J. Sjogren, M. Ugander, M. Carlsson, H. Engblom, and H. Arheden. Design and validation of Segment–freely available software for cardiovascular image analysis. *BMC Med. Imaging* 10:1, 2010.

[15] Hong, J. M., C. S. Chung, O. Y. Bang, S. W. Yong, I. S. Joo, and K. Huh. Vertebral artery dominance contributes to basilar artery curvature and peri-vertebrobasilar junctional infarcts. *J. Neurol. Neurosurg. Psychiatr.* 80:1087–1092, 2009.

[16] Jozwik, K., and D. Obidowski. Numerical simulations of the blood flow through vertebral arteries. *J. Biomech.* 43:177–185, 2010.

[17] Ku, D. N. Blood flow in arteries. *Annu. Rev. Fluid Mech.* 29:399–434, 1997.

[18] Ku, D. N., D. P. Giddens, C. K. Zarins, and S. Glagov. Pulsatile flow and atherosclerosis in the human carotid bifurcation—positive correlation between plaque location and low and oscillating shear-stress. *Arteriosclerosis* 5:293–302, 1985.

[19] Labropoulos, N., P. Nandivada, and K. Bekelis. Prevalence and impact of the subclavian steal syndrome. *Ann. Surg.* 252:166–170, 2010.

[20] Lee, S. W., L. Antiga, and D. A. Steinman. Correlations among indicators of disturbed flow at the normal carotid bifurcation. *J. Biomech. Eng.* 131:061013, 2009.

[21] Malek, A. M., S. L. Alper, and S. Izumo. Hemodynamic shear stress and its role in atherosclerosis. *JAMA* 282:2035–2042, 1999.

[22] Morbiducci, U., R. Ponzini, M. Grigioni, and A. Redaelli. Helical flow as fluid dynamic signature for atherogenesis risk in aortocoronary bypass. A numeric study. *J. Biomech.* 40:519–534, 2007.

[23] Morbiducci, U., D. Gallo, D. Massai, F. Consolo, R. Ponzini, L. Antiga, C. Bignardi, M. A. Deriu, and A. Redaelli. Outflow conditions for image-based hemodynamic models of the carotid bifurcation: implications for indicators of abnormal flow. *J. Biomech. Eng.* 132:091005, 2010.

[24] Moyle, K. R., L. Antiga, and D. A. Steinman. Inlet conditions for image-based CFD models of the carotid bifurcation: is it reasonable to assume fully developed flow? *J. Biomech. Eng.* 128:371–379, 2006.

[25] Osiro, S., A. Zurada, J. Gielecki, M. M. Shoja, R. S. Tubbs, and M. Loukas. A review of subclavian steal syndrome with clinical correlation. *Med. Sci. Monit.* 18(5):RA57–RA63, 2012.

[26] Papaharilaou, Y., N. Aristokleous, I. Seimenis, M. I. Khozeymeh, G. C. Georgiou, B. C. Brott, E. Eracleous, and A. S. Anayiotos. Effect of head posture on the healthy human carotid bifurcation hemodynamics. *Med. Biol. Eng. Comput.* 51:207–218, 2013.

[27] Peluso, J. P., W. J. van Rooij, M. Sluzewski, and G. N. Beute. Aneurysms of the vertebrobasilar junction: incidence, clinical presentation, and outcome of endovascular treatment. *AJNR Am. J. Neuroradiol.* 28:1747–1751, 2007.

[28] R. Core Team. R: A Language and Environment for Statistical Computing. R Foundation for Statistical Computing, Vienna, Austria, http://www.R-project.org/.

[29] Ravensbergen, J., J. W. Ravensbergen, J. K. B. Krijger, B. Hillen, and H. W. Hoogstraten. Localizing role of hemodynamics in atherosclerosis in several human vertebrobasilar junction geometries. *Arterioscler. Thromb. Vasc. Biol.* 18:708–716, 1998.

[30]Ross, R. Atherosclerosis is an inflammatory disease. *Am. Heart J.* 138:S419–S420, 1999.

[31]Sakaguchi, M., K. Kitagawa, H. Hougaku, H. Hashimoto, Y. Nagai, H. Yamagami, T. Ohtsuki, N. Oku, K. Hashikawa, K. Matsushita, M. Matsumoto, and M. Hori. Mechanical compression of the extracranial vertebral artery during neck rotation. *Neurology* 61:845–847, 2003.

[32]Steinman, D. A., and C. A. Taylor. Flow imaging and computing: large artery hemodynamics. *Ann. Biomed. Eng.* 33:1704–1709, 2005.

[33]Thomas, J. B., L. Antiga, S. L. Che, J. S. Milner, D. A. Steinman, J. D. Spence, and B. K. Rutt. Variation in the carotid bifurcation geometry of young versus older adults: implications for geometric risk of atherosclerosis. *Stroke* 36:2450–2456, 2005.

[34]Yushkevich, P. A., J. Piven, H. C. Hazlett, R. G. Smith, S. Ho, J. C. Gee, and G. Gerig. User-guided 3D active contour segmentation of anatomical structures: significantly improved efficiency and reliability. *Neuroimage* 31:1116–1128, 2006.